Research Article | Vol. 29, No. 17 / 16 August 2021 / Optics Express 27004
Optics EXPRESS

8 fs laser pulses from a compact gas-filled multi-pass cell

P. Rueda,[1,2] F. Videla,[1,3] T. Witting,[2] G. A. Torchia,[1] and F. J. Furch[2,*]

[1]Centro de Investigaciones Ópticas (CIOp) CONICET La Plata-CICBA, Camino Centenario y 506 s/n, M.B. Gonnet, CP 1897, Provincia de Buenos Aires, Argentina
[2]Max Born Institute for Nonlinear Optics and Short Pulse Spectroscopy, Max-Born-Str. 2A 12489, Berlin, Germany
[3]Departamento de Ciencias Básicas, Facultad de Ingeniería UNLP, 1 y 47 La Plata, Argentina
*furch@mbi-berlin.de

Abstract: Compression of 42 fs, 0.29 mJ pulses from a Ti:Sapphire amplifier down to 8 fs (approximately 3 optical cycles) is demonstrated by means of spectral broadening in a compact multi-pass cell filled with argon. The efficiency of the nonlinear pulse compression is limited to 45 % mostly by losses in the mirrors of the cell. The experimental results are supported by 3-dimensional numerical simulations of the nonlinear pulse propagation in the cell that allow us to study spatio-spectral properties of the pulses after spectral broadening.

1. Introduction

In recent years a great deal of effort has been devoted to generate few-cycle laser pulses with moderate to high energies (few-µJ to few-mJ). Potential applications include, but are not limited to, the study of ultrafast processes in light-matter interaction in the domain of Attosecond Science [1], strong field physics [2] and novel methods of laser material processing [3]. Chirped pulse amplification (CPA) provides energy scaling through the amplification of ultrashort pulses from mode-locked laser oscillators. However, the amplified pulse duration is limited by gain-narrowing effects during the amplification process. Nonlinear pulse compression, based on pulse spectral broadening during nonlinear pulse propagation dominated by self-phase modulation (SPM), offers an alternative to circumvent this limitation.

Many techniques have been proposed and demonstrated for the nonlinear compression of laser pulses [4]. In particular, the combination of Ti:Sapphire CPAs and spectral broadening in gas-filled hollow-core fibers (HCF) [5] has lead to the generation of sub-4 fs pulses (approximately 1.5 optical cycles around 800 nm) with multi-mJ pulse energy [6,7]. Meanwhile, spectral broadening in HCFs of longer pulses from CPAs based on direct diode pumping of Yb-doped gain materials, has provided a route to generate 10 fs, 3.18 mJ pulses at 100 kHz repetition rate (318 W average power) at a central wavelength around 1030 nm [8].

Besides the required spectral broadening, HCFs offer minimized space-time couplings [9] and a spatial mode dominated by the fundamental mode propagating in the wave-guiding structure. However, HCFs are prone to optical damage at the entrance of the guiding structure, specially for input pulses combining high peak and average power. Hence, they are sensitive to pointing instabilities. Nevertheless, the output of a HCF provides a beam stable in position and pointing, which is useful for applications. In contrast, for any spectral broadening alternative technique that is insensitive to beam pointing instabilities, pointing instability issues must be addressed before integration of the compressed pulses into an application. Multi-plate super-continuum generation (MPSC) [10] is a simple alternative to HCFs that is impervious to beam pointing instabilities. MPSC has been implemented to post-compress few-cycle pulses from a high power, high repetition rate optical parametric chirped pulse amplification system (OPCPA) down to

#435086 https://doi.org/10.1364/OE.435086
Journal © 2021 Received 24 Jun 2021; revised 28 Jul 2021; accepted 28 Jul 2021; published 4 Aug 2021

Optics EXPRESS

the single cycle limit [11] or to compress pulses from an Yb-based CPA from > 100 fs down to the single-cycle limit [12]. Although MPSC constitutes a simple and affordable method for generating few-cycle pulses, the resulting pulses may present certain degree of spatio-temporal distortions [11].

In 2016 Schulte *et al.* introduced a robust strategy for nonlinear compression of 100 fs - 1 ps pulses at around 1 µm from laser amplifiers or high power oscillators known as multi-pass cell (MPC) [13] . The original idea placed a glass window, responsible for SPM, at the position of the beam waist in a Herriot-type delay-line or cell built with high reflectivity mirrors. The idea was later extended to cells inside chambers filled with noble gases. The pulse travels through the Herriot-cell multiple times with only minor losses and a controlled amount of SPM per pass through the position of the waist. The accumulated nonlinear phase after many round trips provides the required spectral broadening for pulse compression. Meanwhile, multiple passes through the cavity are responsible for maintaining the beam quality and homogenizing the spatio-temporal distribution, if the B-integral [14] per pass is kept rather low [15]. In particular, if the B-integral per pass is low, in a first approximation the Kerr-lens effect can be neglected and the propagation can be modelled by Gaussian beam propagation and a 1-Dimensional model accounting for SPM [16]. The technique has been successfully applied to compress pulses from a variety of systems, most notably, for the compression of ps and sub-ps pulses down to a few tens of fs at extremely high average powers reaching 1 kW, with high efficiency exceeding 90 % [17–20].

Although multi-pass cells have shown remarkable performance, especially for compression of sub-ps pulses at high-average-power to sub-50 fs, extension to the few-cycle regime presents additional challenges. As indicated by Nagy *et al.* [4], in order to maintain high efficiency and low B-integral per pass, cavity mirrors must necessarily support near octave-spanning spectral range with high reflectivity (well above 99 %) and low group delay dispersion (GDD), while exhibiting high damage threshold, in order to keep the size of the cell reasonable. To bridge this gap, compression in MPC has been combined with a second compression stage using a different approach [21,22]. In addition, a two-stage MPC compression approach has been implemented by Balla *et al.* to demonstrate the compression of ps pulses at 1030 nm down to 13 fs [23]. Moreover, Müller *et al.* have recently demonstrated the compression of 200 fs, 1 mJ pulses at 500 kHz at 1030 nm from a fiber CPA down to 6.9 fs utilizing a two-stage compression approach [24]. In this particular case, the second MPC incorporates a complex array of dielectrically-enhanced silver mirrors that offer improved reflectivity over a broad bandwidth with minimized GDD. Due to the extremely high average power and the absorption in the silver coatings, active cooling of the mirrors inside the chamber had to be implemented. Furthermore, Cao *et al.* have numerically studied the implementation of MPCs for the compression of 30 fs pulses at 800 nm to the few-cycle regime, with radial and azimuthal input polarization [25] and Laguerre-Gaussian spatial modes [26].

In this work, a compact MPC setup with moderately high B-integral per round-trip is implemented to post-compress nearly transform-limited 42 fs pulses from a Ti:Sapphire CPA. Pulse compression down to 8 fs is demonstrated with a pulse energy of 130 µJ. The experimental results are complemented by numerical simulations in order to estimate the residual space-time couplings. The results presented here represent an interesting alternative approach for the post-compression of pulses from high repetition rate OPCPAs with similar energy [27–35].

2. Experimental setup

The experimental setup is shown in Fig. 1. A commercial Ti:Sapphire CPA system (Spectra-Physics, Spitfire) delivered 42 fs pulses at a central wavelength of 790 nm with energy up to 3 mJ and repetition rate of 1 kHz. A $\lambda/2$ wave plate and a pair of thin-film polarizers control the input energy into the compression setup. A Galilean telescope and a focusing plano-convex lens (f =

Optics EXPRESS

500 mm) were utilized to match the beam size and wavefront to the eigen-mode of the cavity in the MPC.

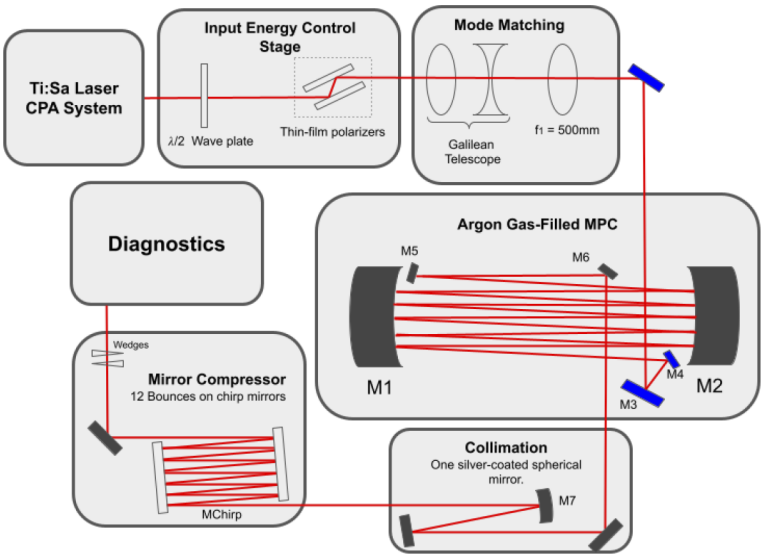

Fig. 1. Multi-pass cell experimental setup configuration. M1, M2: cavity mirrors. M3, M4: dielectric turning mirrors. M5, M6: silver-coated turning mirrors. M7: silver-coated spherical mirror. MChirp: Chirped mirrors.

The MPC was contained in a compact chamber (65 cm x 30 cm x 30 cm) filled with a gas of Ar atoms. The top cover of the chamber consisted of a 5 cm thick clear Plexiglass block for visual inspection purposes. The cavity was built with two silver-coated spherical mirrors (radius = 300 mm, diameter = 50 mm) separated by a distance of 584 mm (mirrors M1 and M2 in Fig. 1). One of the mirrors was mounted on a linear translation stage in order to fine-tune the cavity length. The beam entered the chamber through a 1 mm thick fused-silica window with an anti-reflection coating. Two dielectric multi-layer steering mirrors (M3 and M4 in Fig. 1), one of them with a diameter of 12.5 mm were utilized to inject the beam into the MPC cavity. The same combination of mirrors, but with silver coatings, was utilized to eject the beam out of the cell after 11 passes through the focal plane of the cavity, and then out of the chamber (M5 and M6 in Fig. 1). The spectrally broadened beam exited the chamber through a 0.5 mm thick uncoated fused-silica window. Under these conditions, the losses through the experimental chamber amounted to 38.6 %. Outside the chamber the beam was collimated using a silver-coated spherical mirror (M7 in Fig. 1). A set of chirped mirrors (Ultrafast Innovations, PC-70) in combination with thin fused-silica wedges were used for dispersion compensation.

3. Results and discussion

For the given cavity length, the input pulse energy was limited to a safe value to avoid damage of the optical components inside the chamber. The pressure of the gas was slowly increased (starting from a few mbar) while monitoring the output spectrum. Both, the gas pressure in the chamber and the distance between the gratings in the compressor of the Ti:Sapphire CPA were optimized to maximize the spectral broadening. In order to avoid significant ionization around the focal plane of the cavity, the input pulse energy was reduced whenever necessary while monitoring visually the focal region of the cavity (to avoid strong plasma formation) and instabilities in the output spectrum. A typical evolution of the spectral broadening as the pressure of Ar in the

Optics EXPRESS

chamber was increased is shown in Fig. 2. All the spectra were taken at a constant pulse energy of 290 µJ at the input of the MPC cavity. As the pressure increases the spectral broadening is characterized by a modulation in the spectrum typical of SPM-induced broadening. In addition, the effect of self-steepening is observed in the progressive blue shifting of the spectrum.

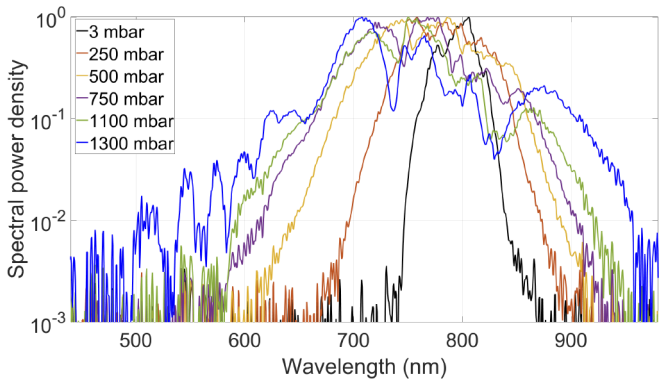

Fig. 2. Evolution of spectral broadening with increasing pressure in the chamber containing the multi-pass cell, shown in a logarithmic scale. In all measurements the pulse energy entering the MPC cavity was 290 µJ.

Upon scanning over different combinations of input energy, input pulse chirp and Ar pressure, optimum spectral broadening with a maximum input energy of (290 ± 10) µJ (at the first cavity mirror), was found for a pressure of 1500 mbar and a mirror separation of 584 mm. After dispersion compensation with 12 bounces off the chirped mirrors and propagation through the fused-silica wedges, the compressed pulses were characterized with a commercial SPIDER (APE GmbH, FC-SPIDER). The resulting spectrum and reconstructed pulse are shown in Fig. 3. Figure 3(a) shows a comparison between the input (dashed light blue line) and the output (solid blue line) spectra. The input pulse was characterized at the output of the CPA with a different commercial SPIDER (APE GmbH, LX-SPIDER). A bigger than 6-fold increase in the pulse spectral width (measured at 1/e of the maximum) is observed. The red curve in the same figure (with corresponding red axis on the right) shows the retrieved spectral phase after dispersion compensation. Due to the limited spectral range of the detector, the spectrum is cut below 547 nm. However, the spectral power density below 600 nm is more than 2 orders of magnitude weaker than at the maximum, and therefore does not affect significantly the results of the pulse characterization. The reconstructed pulse (solid blue line) is presented in Fig. 3(b), where it is compared to the input pulse (dashed light blue line) and the Fourier-transform limited pulse (dashed blue line) corresponding to the broadened spectrum. The pulse duration of 8.06 fs Full-Width at Half Maximum (FWHM) represents 1.6 times the Fourier-transform limited pulse duration (5.0 fs) and 3.1 optical cycles within the FWHM. A residual third order term in the spectral phase prevents from achieving compression closer to the Fourier-transform limit. After losses in the chirped-mirror compressor and several steering mirrors, the pulse energy was reduced another 26 % resulting in a compressed pulse energy of (130 ± 10) µJ. The total efficiency in the setup is estimated then at 45.5 %.

For the spectrally broadened pulses presented in Fig. 3, the beam at the output of the experimental chamber was characterized before the chirped mirror compressor with a commercial beam profiler (Thorlabs Inc., BC106N-VIS). Figure 4(a) shows the color-coded intensity spatial distribution of the collimated beam in a scale normalized to the maximum number of counts in the image. The image was integrated over the y- and x-axis to construct the profiles shown in Fig. 4(c). In Fig. 4(b) the focused beam is shown at the focal plane of a 400 mm focal length

Optics EXPRESS

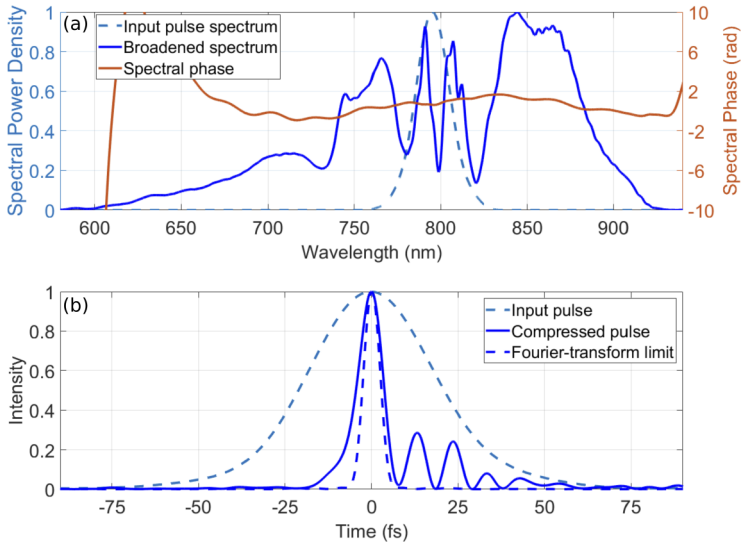

Fig. 3. (a) Measured spectrum (solid blue) and retrieved spectral phase (red). The spectrum of the input pulse is shown for comparison (dashed light blue). (b) Retrieved pulse (squared absolute value of the pulse envelope) and Fourier-transform limited pulse (solid and dashed blue respectively). The measured input pulse is also shown for comparison (dashed light blue).

plano-convex lens. In the focal plane the beam is homogeneous and round, with no visible significant low energy pedestals compromising the achievable intensity. The spatial distribution was integrated to construct the beam profiles along the x- and y-axis shown in Fig. 4(d).

In order to quantify this description of the focused beam, the amount of energy in low intensity pedestals in the spatial distribution of Fig. 4(b) was estimated. In order to do so, the spatial distribution was integrated within a circle centered around the beam (dashed red circle in Fig. 4(b)), and with a diameter equal to π times the average of the beam widths (e^{-2} of the maximum intensity) in x and y. This region would contain approximately 99 % of the energy for a Gaussian beam. The ratio between this integral and an integration over the full spatial distribution gives an estimation of the content of energy in low intensity pedestals for non-ideal beams. The region within the circle in Fig. 4(b)) contains 85 % of the energy. In other words, 15 % of the pulse energy is lost to the spatial low energy pedestal.

One of the attractive properties of the MPC technique is the fact that the combination of a slow build-up of nonlinear phase and propagation in the cavity results in a homogeneous spatio-temporal (or spatio-spectral) distribution [15]. Typically the B-integral per pass in the cell is limited to relatively small values ($< \pi$) in order to prevent space-time couplings. The B-integral per round trip in the setup can be estimated with a simple expression derived by Hanna *et al.* [15]:

$$B_{\mathrm{RoundTrip}} = \pi \frac{P_{\mathrm{peak}}}{P_{\mathrm{crit}}} \arctan \sqrt{\frac{L}{2R - L}}. \tag{1}$$

Here P_{peak} is the pulse peak power, P_{crit} is the critical power for self-focusing, L is separation between the cavity mirrors (assumed to be identical) and R their radii of curvature. In the present case, $B_{\mathrm{RoundTrip}}$ was estimated to be approximately equal to $1.5 \times \pi$. Therefore, it is instructive to study the spatio-spectral distribution of the output pulses.

Figure 5(a) shows the broadened spectra at different positions across the beam. The spectra were taken in the same plane where the image of Fig. 4(a) was taken, by displacing an optical

Optics EXPRESS

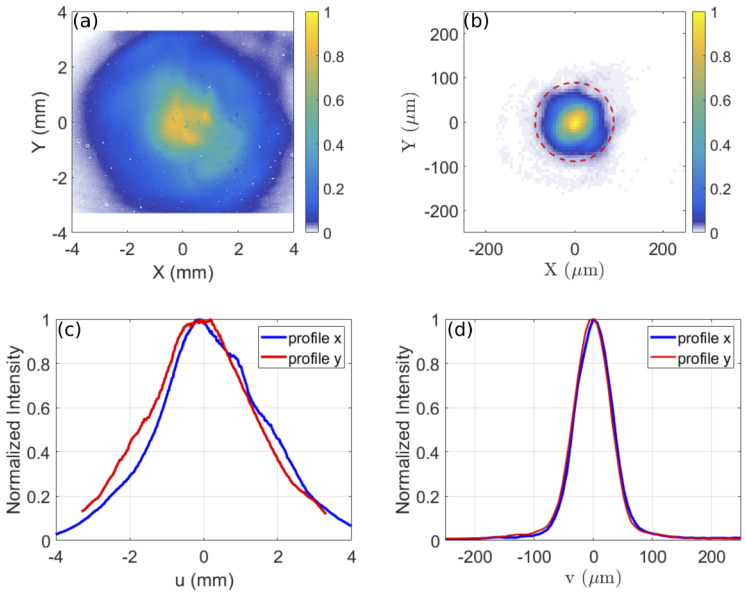

Fig. 4. (a) Collimated beam before the chirp-mirror compressor. (b) Focused beam measured in the focal plane of a 400 mm focal length lens. The red dashed circle indicates the region of integration for an estimation of the energy in the main part of the beam. (c) Beam profiles extracted from integrating the beam in (a) in the *y*-axis (profile x) and in the *x*-axis (profile y). u represents either the *x*- or *y*-axis. (d) Beam profiles (solid lines) extracted from integrating the spatial distribution in (b) along the horizontal and vertical directions (profile y and profile x respectively). v represents either the *x*- or *y*-axis.

fiber coupled to a spectrometer across the beam profile, utilizing a micrometer stage. Figure 5(b) shows the Fourier-transform limited (FTL) pulse duration corresponding to the spectra in Fig. 5(a). The pulse duration is relatively constant within the FWHM of the beam profile (approximately between -1.5 mm and 1.5 mm). Towards the edges of the beam the FTL is shorter, but the signal to noise ratio of the spectra is lower. Overall, although there is a mild dependence of the broadened spectrum and the FTL on the position across the beam, compression to few-cycle pulses is supported across the entire beam profile. Note that the shape of the spectra in Fig. 5(a) differs from the SPIDER measurement in Fig. 3(a). These data sets were taking during different days and the input pulse shape into the MPC setup differed from day to day due to long term instabilities in the Ti:Sapphire CPA.

In order to better understand the impact of the relatively high B-integral per round trip, numerical simulations were performed to qualitatively reproduce the spectral broadening observed in Fig. 3(a). To simulate the propagation through the MPC a 3D+1 nonlinear propagation equation was derived for the pulse envelope under the Slowly Evolving Wave Approximation [36]. The equation was solved on a 200x200x512 (x, y, t) grid applying a split-step method in which dispersion and diffraction are described in the frequency-domain, while SPM and self-steepening are applied in the time-domain. The nonlinear coefficient was assumed constant over the entire spectral region. The value of the nonlinear coefficient was taken from measured values published in the literature [37]. The input beam profile was assumed to be Gaussian with the size and wave front curvature matching the mode of the cavity, while the temporal shape was taken from the measurement of the input pulse with the LX-SPIDER. The radii of curvature of the mirrors, mirror separation, gas pressure and pulse energy were taken from the experimental values quoted above. A mirror reflectivity of 97 % with a flat spectral response was assumed, corresponding

Optics EXPRESS

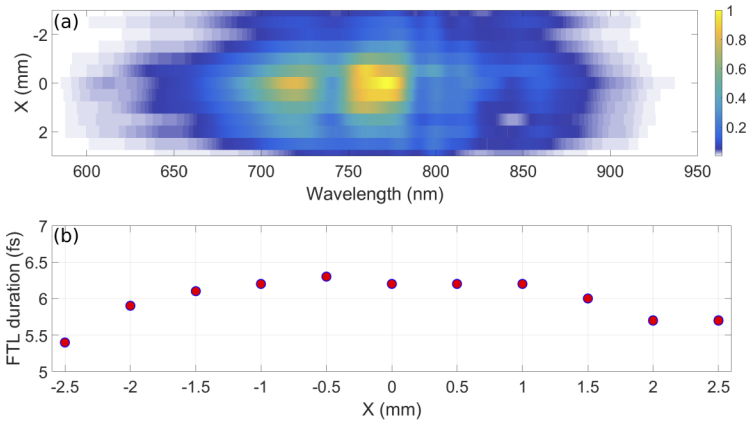

Fig. 5. (a) Spatio-spectral distribution measured along the horizontal coordinate. (b) Fourier-transform limited pulse duration for the spectra shown in (a).

to the protected-silver coatings of the mirrors used in the experiment. The input energy was multiplied by a dimensionless parameter between 0 and 1 that was used to account for pulse pedestals, wave front aberrations, etc., effectively degrading the peak intensity. This was the only variable parameter of the model and it was adjusted in order to approximately reproduce the experimental spectrum. For the results shown below this factor was set to 0.5. A summary of the simulation results is presented in Fig. 6.

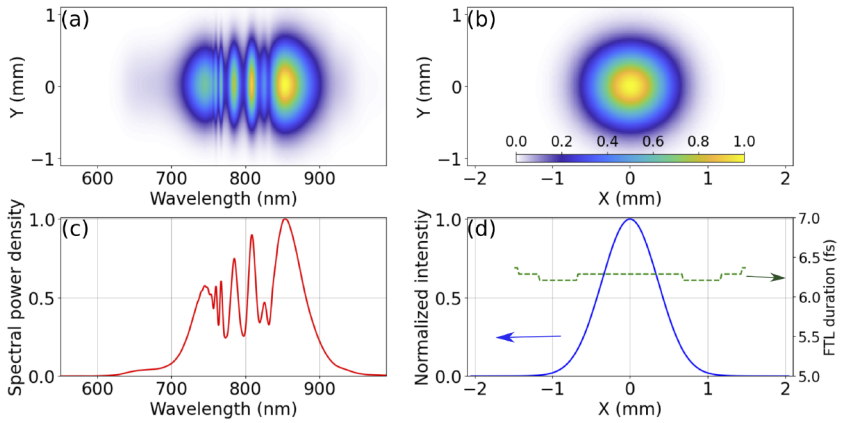

Fig. 6. Summary of simulation results. (a) Spatio-spectral distribution integrated along one spatial dimension. (b) Output beam. (c) Spatially-integrated spectrum. (d) Output beam profile (solid blue line) obtained by integrating the beam in (b) along the vertical (y-axis) direction. The dashed green line shows the FTL pulse duration as a function of position.

Figure 6(a) shows the spatio-spectral distribution integrated over one of the spatial coordinates. The results clearly show a dependence of the spectrum with position. The spectrum obtained by integrating along both spatial coordinates is shown in Fig. 6(c). Although the simulated spectrum reproduces qualitatively some of the features of the experimental spectrum shown in Fig. 3, it does not reproduce it exactly. In particular the experimental spectrum is slightly more blue-shifted, a sign that ionization may be playing an important role. A one-to-one comparison is challenging, since a fraction of the beam is sampled with the input iris of the SPIDER. Figure 6(b) shows the output beam at the position of the cavity mirror. A profile calculated by integrating

Optics EXPRESS

along the *y*-axis is shown in Fig. 6(d) (solid blue line). Additionally, the FTL pulse duration as a function of position is included (dashed green line). The achievable pulse duration is practically constant across the beam profile. No signs of beam degradation are observed in the simulation. The code implements an estimation of the beam profile at each step during the propagation that allows comparing the beam size with the calculated Gaussian mode in the cavity. The perturbation introduced by self-focusing decreases the size of the beam on the mirrors for some of the round trips, effectively limiting the input pulse energy due potential damage to the mirrors. The amount of space-time couplings can be quantified by a parameter indicating how the beam properties depend on the spectral component, according to the definitions of Hanna *et al.* [15]. The spatio-temporal couplings are considered negligible if this quantity is below 0.1. For the distribution shown in Fig. 6, the space-time coupling parameter amounts to 0.23, reflecting the fact that the spatio-temporal distortions are not negligible.

A quantity similar to a Strehl ratio can be calculated to estimate the effects of the space-time couplings on the achievable peak intensity: a ratio of the intensity at focus of the compressed pulse with spatio-temporal distortions, to the intensity of a distortion-free pulse calculated from the distorted one, according to the definition given by Giree *et al.* [38]. This ratio varies between 0 and 1, with 1 corresponding to a space-time coupling-free field. For the simulated field shown in Fig. 6, the beam was numerically collimated with an ideal lens and then focused with a second ideal lens of focal length 500 mm. The corresponding ratio due to spatio-temporal distortions amounts to 0.91. Therefore, it can be concluded that although the space-time couplings are not negligible, their effect on the peak intensity is not dramatic for the case considered here.

The results presented in Fig. 6 and its corresponding discussions suggest that under our experimental conditions, a careful spatio-temporal analysis of the compressed pulses [9,39,40] is advisable. A straightforward alternative to the scheme presented here is to replace the silver coatings in the cavity mirrors (and elsewhere) by silver plus a thin dielectric multi-layer coating that enhances the reflectivity over the full bandwidth (reflectivity $\approx 98.5\%$) with minimum group delay dispersion. In that case, the number of round trips could be increased to 11 keeping approximately the same transmission through the MPC setup but lowering the B-integral per round trip (by lowering the gas pressure), or the efficiency of the setup can be increased keeping similar conditions to the experiment presented here.

4. Conclusions

In summary, we have demonstrated the compression of sub-45 fs pulses at 800 nm down to 8 fs (3.1 cycles) in a gas-filled multi-pass cell for an input pulse energy of almost 300 µJ. In order to avoid significant losses while keeping a broad bandwidth, the B-integral per round trip in the cell had to be set at relatively high values reaching $1.5 \times \pi$, which in turn resulted in non-negligible space-time couplings. However, it was shown that all the spectra measured at different positions across the beam profile support compression to few-cycle pulses. The experimental results were supported by 3D+1 numerical simulations that confirm the presence of space-time couplings limiting the achievable peak intensity. In future experiments all silver mirrors will be replaced by dielectrically enhanced silver mirrors. In combination with a broadband anti-reflection coated output window, these modifications should allow the compression of pulses with few-hundred µJ of energy with more than 50 % efficiency in a compact setup. This could be particularly attractive for the nonlinear compression of pulses from high power, high repetition rate OPCPA systems with similar pulse energies.

Funding. Horizon 2020 Framework Programme (871124); Consejo Nacional de Investigaciones Científicas y Técnicas (PUE 22920170100016CO); Agencia Nacional de Promoción Científica y Tecnológica (PICT-2016-4086).

Acknowledgments. The authors would like to acknowledge Christoph Reiter for technical support and Tamas Nagy for fruitful discussions. This project has received funding from the European Union's Horizon 2020 research and innovation programme under grant agreement no. 871124 Laserlab-Europe. This work was partially supported by the

Optics EXPRESS

Agencia de Promoción Científica y Tecnológica under project PICT-2016-4086 and by CONICET under PUE grant no. 22920170100016CO.

Disclosures. The authors declare no conflicts of interest.

Data availability. Data underlying the results presented in this paper are not publicly available at this time but may be obtained from the authors upon reasonable request.

References

1. F. Krausz and M. Ivanov, "Attosecond physics," Rev. Mod. Phys. **81**(1), 163–234 (2009).
2. N. Camus, B. Fischer, M. Kremer, V. Sharma, A. Rudenko, B. Bergues, M. Kübel, N. G. Johnson, M. F. Kling, T. Pfeifer, J. Ullrich, and R. Moshammer, "Attosecond correlated dynamics of two electrons passing through a transition state," Phys. Rev. Lett. **108**(7), 073003 (2012).
3. F. J. Furch, W. D. Engel, T. Witting, A. Perez-Leija, M. J. J. Vrakking, and A. Mermillod-Blondin, "Single-step fabrication of surface waveguides in fused silica with few-cycle laser pulses," Opt. Lett. **44**(17), 4267–4270 (2019).
4. T. Nagy, P. Simon, and L. Veisz, "High-energy few-cycle pulses: post-compression techniques," Adv. Phys.: X **6**(1), 1845795 (2021).
5. M. Nisoli, S. D. Silvestri, O. Svelto, R. Szipöcs, K. Ferencz, C. Spielmann, S. Sartania, and F. Krausz, "Compression of high-energy laser pulses below 5 fs," Opt. Lett. **22**(8), 522–524 (1997).
6. F. Böhle, M. Kretschmar, A. Jullien, M. Kovacs, M. Miranda, R. Romero, H. Crespo, U. Morgner, P. Simon, R. Lopez-Martens, and T. Nagy, "Compression of CEP-stable multi-mJ laser pulses down to 4 fs in long hollow fibers," Laser Phys. Lett. **11**(9), 095401 (2014).
7. T. Nagy, M. Kretschmar, M. J. J. Vrakking, and A. Rouzée, "Generation of above-Terawatt 1.5-cycle visible pulses at 1 kHz by post-compression in a hollow fiber," Opt. Lett. **45**(12), 3313–3316 (2020).
8. T. Nagy, S. Hädrich, P. Simon, A. Blumenstein, N. Walther, R. Klas, J. Buldt, H. Stark, S. Breitkopf, P. Jójárt, I. Seres, Z. Várallyay, T. Eidam, and J. Limpert, "Generation of three-cycle multi-millijoule laser pulses at 318 W average power," Optica **6**(11), 1423–1424 (2019).
9. T. Witting, F. Frank, C. A. Arrell, W. A. Okell, J. P. Marangos, and J. W. G. Tisch, "Characterization of high-intensity sub-4-fs laser pulses using spatially encoded spectral shearing interferometry," Opt. Lett. **36**(9), 1680–1682 (2011).
10. C.-H. Lu, Y.-J. Tsou, H.-Y. Chen, B.-H. Chen, Y.-C. Cheng, S.-D. Yang, M.-C. Chen, C.-C. Hsu, and A. H. Kung, "Generation of intense supercontinuum in condensed media," Optica **1**(6), 400–406 (2014).
11. C.-H. Lu, T. Witting, A. Husakou, M. J. Vrakking, A. H. Kung, and F. J. Furch, "Sub-4 fs laser pulses at high average power and high repetition rate from an all-solid-state setup," Opt. Express **26**(7), 8941–8956 (2018).
12. C.-H. Lu, W.-H. Wu, S.-H. Kuo, J.-Y. Guo, M.-C. Chen, S.-D. Yang, and A. H. Kung, "Greater than 50 times compression of 1030 nm Yb:KGW laser pulses to single-cycle duration," Opt. Express **27**(11), 15638–15648 (2019).
13. J. Schulte, T. Sartorius, J. Weitenberg, A. Vernaleken, and P. Russbueldt, "Nonlinear pulse compression in a multi-pass cell," Opt. Lett. **41**(19), 4511–4514 (2016).
14. A. E. Siegman, Lasers (University Science Books, 1986).
15. M. Hanna, X. Délen, L. Lavenu, F. Guichard, Y. Zaouter, F. Druon, and P. Georges, "Nonlinear temporal compression in multipass cells: theory," J. Opt. Soc. Am. B **34**(7), 1340–1347 (2017).
16. N. Daher, F. Guichard, S. W. Jolly, X. Delen, F. Quere, M. Hanna, and P. Georges, "Multipass cells: 1D numerical model and investigation of spatio-spectral couplings at high nonlinearity," J. Opt. Soc. Am. B **37**(4), 993–999 (2020).
17. M. Ueffing, S. Reiger, M. Kaumanns, V. Pervak, M. Trubetskov, T. Nubbemeyer, and F. Krausz, "Nonlinear pulse compression in a gas-filled multipass cell," Opt. Lett. **43**(9), 2070–2073 (2018).
18. P. Russbueldt, J. Weitenberg, J. Schulte, R. Meyer, C. Meinhardt, H. D. Hoffmann, and R. Poprawe, "Scalable 30 fs laser source with 530 W average power," Opt. Lett. **44**(21), 5222–5225 (2019).
19. C. Grebing, M. Müller, J. Buldt, H. Stark, and J. Limpert, "Kilowatt-average-power compression of millijoule pulses in a gas-filled multi-pass cell," Opt. Lett. **45**(22), 6250–6253 (2020).
20. M. Kaumanns, V. Pervak, D. Kormin, V. Leshchenko, A. Kessel, M. Ueffing, Y. Chen, and T. Nubbemeyer, "Multipass spectral broadening of 18 mJ pulses compressible from 1.3 ps to 41 fs," Opt. Lett. **43**(23), 5877–5880 (2018).
21. L. Lavenu, M. Natile, F. Guichard, X. Délen, M. Hanna, Y. Zaouter, and P. Georges, "High-power two-cycle ultrafast source based on hybrid nonlinear compression," Opt. Express **27**(3), 1958–1967 (2019).
22. C.-L. Tsai, F. Meyer, A. Omar, Y. Wang, A.-Y. Liang, C.-H. Lu, M. Hoffmann, S.-D. Yang, and C. J. Saraceno, "Efficient nonlinear compression of a mode-locked thin-disk oscillator to 27 fs at 98 W average power," Opt. Lett. **44**(17), 4115–4118 (2019).
23. P. Balla, A. B. Wahid, I. Sytcevich, C. Guo, A.-L. Viotti, L. Silletti, A. Cartella, S. Alisauskas, H. Tavakol, U. Grosse-Wortmann, A. Schönberg, M. Seidel, A. Trabattoni, B. Manschwetus, T. Lang, F. Calegari, A. Couairon, A. L'Huillier, C. L. Arnold, I. Hartl, and C. M. Heyl, "Postcompression of picosecond pulses into the few-cycle regime," Opt. Lett. **45**(9), 2572–2575 (2020).
24. M. Müller, J. Buldt, H. Stark, C. Grebing, and J. Limpert, "Multipass cell for high-power few-cycle compression," Opt. Lett. **46**(11), 2678–2681 (2021).
25. H. Cao, R. S. Nagymihaly, V. Chvykov, N. Khodakovskiy, and M. Kalashnikov, "Multipass-cell-based post-compression of radially and azimuthally polarized pulses to the sub-two-cycle regime," J. Opt. Soc. Am. B **36**(9), 2517–2525 (2019).

Optics EXPRESS

26. H. Cao, R. S. Nagymihaly, and M. Kalashnikov, "Relativistic near-single-cycle optical vortex pulses from noble gas-filled multipass cells," Opt. Lett. **45**(12), 3240–3243 (2020).
27. M. Baudisch, B. Wolter, M. Pullen, M. Hemmer, and J. Biegert, "High power multi-color OPCPA source with simultaneous femtosecond deep-UV to mid-IR outputs," Opt. Lett. **41**(15), 3583–3586 (2016).
28. F. J. Furch, T. Witting, A. Giree, C. Luan, F. Schell, G. Arisholm, C. P. Schulz, and M. J. Vrakking, "CEP-stable few-cycle pulses with more than 190 μJ of energy at 100 kHz from a noncollinear optical parametric amplifier," Opt. Lett. **42**(13), 2495–2498 (2017).
29. S. Hrisafov, J. Pupeikis, P.-A. Chevreuil, F. Brunner, C. R. Phillips, L. Gallmann, and U. Keller, "High-power few-cycle near-infrared OPCPA for soft X-ray generation at 100 kHz," Opt. Express **28**(26), 40145–40154 (2020).
30. J. Matyschok, T. Lang, T. Binhammer, O. Prochnow, S. Rausch, M. Schultze, A. Harth, P. Rudawski, C. L. Arnold, A. L'Huillier, and U. Morgner, "Temporal and spatial effects inside a compact and CEP stabilized, few-cycle OPCPA system at high repetition rates," Opt. Express **21**(24), 29656–29665 (2013).
31. M. Mero, Z. Heiner, V. Petrov, H. Rottke, F. Branchi, G. M. Thomas, and M. J. J. Vrakking, "43 W, 1.55 μm and 12.5 W, 3.1 μm dual-beam, sub-10 cycle, 100 kHz optical parametric chirped pulse amplifier," Opt. Lett. **43**(21), 5246–5249 (2018).
32. M. Neuhaus, H. Fuest, M. Seeger, J. Schötz, M. Trubetskov, P. Russbueldt, H. Hoffmann, E. Riedle, Z. Major, V. Pervak, M. F. Kling, and P. Wnuk, "10 W CEP-stable few-cycle source at 2 μm with 100 kHz repetition rate," Opt. Express **26**(13), 16074–16085 (2018).
33. S. Prinz, M. Haefner, C. Y. Teisset, R. Bessing, K. Michel, Y. Lee, X. T. Geng, S. Kim, D. E. Kim, T. Metzger, and M. Schultze, "CEP-stable, sub-6 fs, 300-kHz OPCPA system with more than 15 W of average power," Opt. Express **23**(2), 1388–1394 (2015).
34. J. Rothhardt, S. Demmler, S. Hädrich, J. Limpert, and A. Tünnermann, "Octave-spanning OPCPA system delivering CEP-stable few-cycle pulses and 22 W of average power at 1 MHz repetition rate," Opt. Express **20**(10), 10870–10878 (2012).
35. N. Thiré, R. Maksimenka, B. Kiss, C. Ferchaud, G. Gitzinger, T. Pinoteau, H. Jousselin, S. Jarosch, P. Bizouard, V. D. Pietro, E. Cormier, K. Osvay, and N. Forget, "Highly stable, 15 W, few-cycle, 65 mrad CEP-noise mid-IR OPCPA for statistical physics," Opt. Express **26**(21), 26907–26915 (2018).
36. A. Couairon, E. Brambilla, T. Corti, D. Majus, O. de J. Ramírez-Góngora, and M. Kolesik, "Practitioner's guide to laser pulse propagation models and simulation," Eur. Phys. J.: Spec. Top. **199**(1), 5–76 (2011).
37. J. K. Wahlstrand, Y.-H. Cheng, and H. M. Milchberg, "High field optical nonlinearity and the Kramers-Kronig relations," Phys. Rev. Lett. **109**(11), 113904 (2012).
38. A. Giree, M. Mero, G. Arisholm, M. J. Vrakking, and F. J. Furch, "Numerical study of spatiotemporal distortions in noncollinear optical parametric chirped-pulse amplifiers," Opt. Express **25**(4), 3104–3121 (2017).
39. M. Miranda, M. Kotur, P. Rudawski, C. Guo, A. Harth, A. L'Huillier, and C. L. Arnold, "Spatiotemporal characterization of ultrashort laser pulses using spatially resolved Fourier transform spectrometry," Opt. Lett. **39**(17), 5142–5145 (2014).
40. G. Pariente, V. Gallet, A. Borot, and O. G. F. Quéré, "Space-time characterization of ultra-intense femtosecond laser beams," Nat. Photonics **10**(8), 547–553 (2016).